Mineralogical Magazine (2019), **83**, 645–654
doi:10.1180/mgm.2019.12

CAMBRIDGE UNIVERSITY PRESS

Article

Lipuite, a new manganese phyllosilicate mineral from the N'Chwaning III mine, Kalahari Manganese Fields, South Africa

Xiangping Gu*[1], Hexiong Yang[2], Xiande Xie[3], Jaco J. van Nieuwenhuizen[4], Robert T. Downs[2] and Stanley H. Evans[2]

[1]School of Geosciences and Info-Physics, Central South University, Changsha, Hunan 410083, China; [2]Department of Geosciences, University of Arizona, 1040 E 4th Street, Tucson, AZ 85721-0077, USA; [3]CAS Key Laboratory of Mineralogy and Metallogeny / Guangdong Provincial Key Laboratory of Mineral Physics and Materials, Guangzhou Institute of Geochemistry, Chinese Academy of Sciences, Guangzhou 510640, China; and [4]Plot 968, Alheit, Kakamas 8870, Northern Cape, South Africa

Abstract

A new phyllosilicate mineral, lipuite (IMA2014-085), has been discovered from the N'Chwaning III mine, Kalahari Manganese Fields, Northern Cape Province, Republic of South Africa. It occurs as platy, tabular, or granular crystals and veined agglomerate in association with Mn-bearing sugilite, taniajacoite, pectolite, richterite, norrishite and namansilite. Lipuite is dark red–brown with vitreous lustre, red streak, an estimated Mohs hardness of 5 and the measured density is 2.83(3) g/cm^3. It is biaxial (+) and characterised by bright red to dark red colour in thin section with measured refractive indices in white light: $\alpha = 1.635(1)$, $\beta = 1.653(1)$, $\gamma = 1.670(1)$ and $2V = 86(2)°$. The Raman spectra of lipuite are composed of over 21 bands at 109, 146, 162, 183, 206, 244, 288, 342, 362, 455, 496, 520, 552, 613, 669, 886, 930, 971, 1097, 3487 and 3540 cm^{-1}. The empirical formula from microprobe analyses is (based on total number of cations = 27.5 and structural refinement): $K_{1.12}Na_{8.16}(Mn_{4.77}Fe_{0.07})_{\Sigma 4.84}Mg_{0.44}[Si_{11.97}O_{30}(OH)_4](PO_4)_{0.94}O_2(OH)_2{\cdot}4H_2O$. The idealised formula is: $KNa_8Mn^{3+}_5Mg_{0.5}[Si_{12}O_{30}(OH)_4](PO_4)O_2(OH)_2{\cdot}4H_2O$.

Lipuite is orthorhombic, space group *Pnnm*, $a = 9.080(3)$, $b = 12.222(3)$, $c = 17.093(5)$ Å, $V = 1897.0(9)$ Å^3 and $Z = 2$. The strongest powder X-ray diffraction peaks [d, Å (*I*) (*hkl*)] are: 9.965(40)(011), 2.938(33)(310), 2.895(100)(311), 2.777(38)(224), 2.713(53)(320), 2.483(32)(126), 2.086(35)(046) and 1.534(40)(446). The crystal structure of lipuite is characterised by sheets of SiO_4 tetrahedra that are linked together along [010] by K^+, Na^+, Mn^{3+}, Mg^{2+} and P^{5+} cations, as well as hydrogen bonds. These tetrahedral sheets consist of 14-membered rings of SiO_4 tetrahedra that zigzag along [100]. The two independent Mn^{3+} cations are both octahedrally coordinated. They form five-membered, edge-shared octahedral clusters between the SiO_4 tetrahedral sheets. Lipuite represents a rather unique structure type and its silicate tetrahedral sheets can be considered a derivative of the silicate sheets in mica.

Keywords: lipuite, phyllosilicate, new mineral, crystal structure, Raman spectrum, Kalahari manganese

(Received 6 September 2018; accepted 22 January 2019; Accepted Manuscript published online: 26 February 2019; Associate Editor: Edward S Grew)

Introduction

The Kalahari Manganese Fields in the North Cape Province of South Africa hosts the largest manganese resource on Earth, ~4 billion tons, accounting for 80% of the mineable manganese ore on land (Beukes, 1983). There are two types of manganese ores present. The low-grade Mamatwan type, making up ~97% of the total reserve, is composed of microcrystalline braunite and kutnohorite lutite and occurs as stratiform beds in the Hotazel Formation of the Paleoproterozoic Transvaal Supergroup. The high-grade Wessels-type ore, constituting mainly of hausmannite, bixbyite, braunite-II, and manganite, was formed from structurally controlled hydrothermal enrichment around 1.0–1.25 Ga (Cairncross and Beukes, 2013; Gutzmer and Beukes, 1996; Dixon, 1989). Since 1981, 24 new minerals discovered in the Kalahari Manganese Fields have been approved by the International Mineralogical Association Commission on New Minerals, Nomenclature and Classification (IMA–CNMNC) (Pasero, 2019) (Table 1), most of which are from the ores of the high-grade Wessels type.

The new mineral, lipuite, is named in honour of the late Chinese geochemist and petrologist, Professor Pu Li (1911–1968). Professor Li received his BSc degree from the Southwest Union University in China in 1942 and PhD from the University of Cambridge in England in 1950. He then became a Professor at the Beijing Institute of Geology and later at the Guiyang Institute of Geochemistry, Chinese Academy of Sciences. Professor Li was the founder and pioneer of isotope geochemistry in China. He also made significant contributions to the development of Chinese geology in general, and petrology in particular. Both the new mineral and its name have been approved by IMA–CNMNC (IMA2014–085, Yang *et al.*, 2015*b*). The cotype sample has been deposited in the collections of the Mineral Museum of the University of Arizona, Tucson, Arizona, USA (UAMM #20010) and the RRUFF Project with deposition number R140946 (http://rruff.info/R140946).

Occurrence and paragenesis

Lipuite was found on a number of specimens collected from the N'Chwaning III mine (part of the Wessels Mine), 27°7′51″S,

*Author for correspondence: Xiangping Gu, Email: guxp2004@163.com
Cite this article: Gu X., Yang H., Xie X., van Nieuwenhuizen J.J., Downs R.T. and Evans S.H. (2019) Lipuite, a new manganese phyllosilicate mineral from the N'Chwaning III mine, Kalahari Manganese Fields, South Africa. *Mineralogical Magazine* **83**, 645–654. https://doi.org/10.1180/mgm.2019.12

Table 1. List of new minerals discovered in the Kalahari Manganese Field.

IMA number*	Name	Ideal formula	Space group	Reference
	Braunite-II	$Ca(Mn^{3+},Fe^{3+})_{14}SiO_{24}$	$I4_1/acd$	de Villiers and Herbstein (1967)
1981–011	Sturmanite	$Ca_6Fe_2^{3+}(SO_4)_{2.5}[B(OH)_4]\ (OH)_{12}{\cdot}25H_2O$	$P3_1c$	Peacor *et al.* (1983)
1988–029	Orlymanite	$Ca_4Mn_3^{2+}Si_8O_{20}(OH)_6{\cdot}2H_2O$	$P\bar{3}$or $P3$	Peacor *et al.* (1990)
1991–031	Vonbezingite	$Ca_6Cu_3(SO_4)_3(OH)_{12}{\cdot}2H_2O$	$P2_1/c$	Dai and Harlow (1992)
1992–033	Hennomartinite	$SrMn^{3+}(Si_2O_7)(OH)_2{\cdot}H_2O$	$Cmcm$	Armbruster *et al.* (1993)
1992–012	Poldervaartite	$(Ca,Mn^{2+})_2[SiO_3(OH)]\ (OH)$	$Pbca$	Dai *et al.* (1993)
1993–036	Effenbergerite	$BaCuSi_4O_{10}$	$P4/ncc$	Giester and Rieck (1994)
1994–002	Nchwaningite	$Mn_2SiO_3(OH)_2{\cdot}H_2O$	$Pca2_1$	Nyfeler *et al.* (1995)
1994–055	Wesselsite	$SrCuSi_4O_{10}$	$P4/ncc;$	Giester and Rieck (1996)
2000–040	Manganvesuvianite	$Ca_{19}Mn\ Al_{10}Mg_2(SiO_4)_{10}(Si_2O_7)_4O(OH)_9$	$P4/n$	Armbruster *et al.* (2002)
2001–014	Tweddillite	$CaSr(Mn^{3+},Fe^{3+})_2Al[Si_3O_{12}](OH)$	$P2_1/m,$	Armbruster *et al.* (2002)
2006–026	Olmiite	$CaMn[SiO_3(OH)](OH)$	$Pbca$	Bonazzi *et al.* (2007)
2009–061	Guidottiite	$(Mn_2Fe^{3+})(SiFe^{3+})O_5(OH)_4$	$P6_3$	Wahle *et al.* (2010)
2012–027	Scottyite	$BaCu_2Si_2O_7$	$Pnma$	Yang *et al.* (2013)
2012–028	Lavinskyite	$K(LiCu)Cu_6(Si_4O_{11})_2(OH)_4$	$Pcnb$	Yang *et al.* (2014)
2012–060	Colinowensite	$BaCuSi_2O_6$	$I4_1/acd$	Rieck *et al.* (2015)
2012–096	Diegogattaite	$Na_2CaCu_2Si_8O_{20}{\cdot}H_2O$	$C2/m$	Rumsey *et al.* (2013)
2012 s.p.	Potassic-mangani-leakeite**	$KNa_2(Mg,Mn^{3+},Fe^{3+},Li)_5Si_8O_{22}(OH)_2$	$P2_1/m$ *or* $P2_1/a$	Hawthorne *et al.* (2012)
2013–012	Cairncrossite	$Sr_2Ca_{7-x}Na_{2x}(Si_4O_{10})_4(OH)_2(H_2O)_{15-x}$	$P\bar{1}$	Giester *et al.* (2016)
2014–085	Lipuite	$KNa_8Mn_5^{3+}Mg_{0.5}[Si_{12}O_{30}(OH)_4](PO_4)O_2(OH)_2{\cdot}4H_2O$	$Pnnm$	This paper
2014–107	Taniajacoite	$SrCaMn_2^{3+}Si_4O_{11}(OH)_4{\cdot}2H_2O$	$C1$	Yang *et al.* (2015a)
2015–009	Meieranite	$Na_2Sr_3MgSi_6O_{17}$	$P2_1nb$	Yang *et al.* (2019)
2015–044	Cyprine	$Ca_{19}Cu^{2+}(Al_{10}Mg_2)Si_{18}O_{68}(OH)_{10}$	$P4/n$	Panikorovskii (2017)

*The data for IMA approval number are from the official website of IMA-CNMNC (Pasero, 2019).
**Potassic-mangani-leakeite was previously named as kornite by Armbruster *et al.* (1993) and redefined by Hawthorne *et al.* (2012)

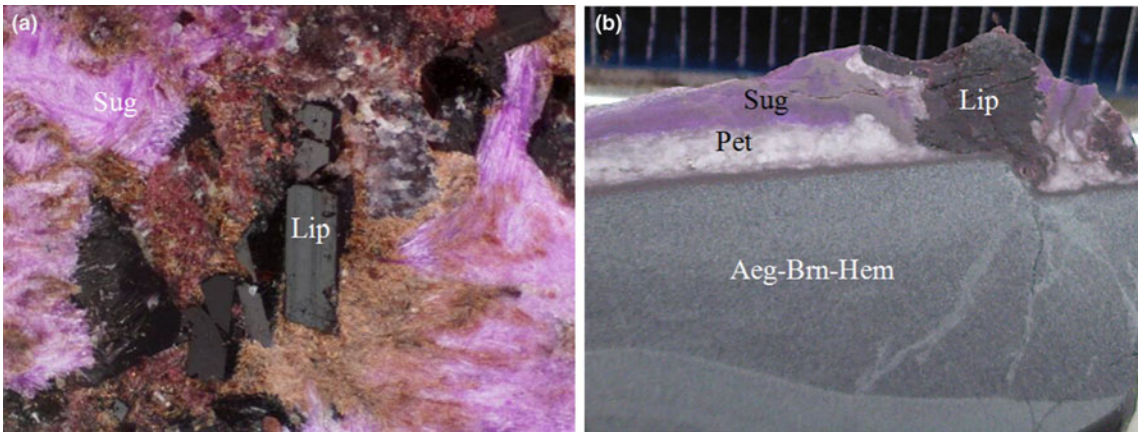

Fig. 1. Occurrence and crystal morphology of lipuite: (*a*) euhedral platy dark crystals of lipuite (Lip) with pink-coloured sugilite (Sug), image width = 2 cm, type specimen R140946 stored in the Mineral Museum of the University of Arizona; (*b*) lipuite–sugilite–pectolite (Pet) crust on microcrystalline aegirine–braunite II–hematite agglomerate (Aeg–Brn–Hem), section vertical to the specimen surface, image width = 2 cm, specimen used to make lpblock07, lpblock08, lpblock09.

22°50′29″E. In the specimens, a crust composed of sugilite–lipuite–pectolite–taniajacoite, 2–5 mm thick, was found on a matrix of aegerine–braunite-II–hematite (Fig. 1). Associated minerals include Mn-bearing sugilite, taniajacoite, pectolite and richterite (Fig. 2*a*, *b*). Norrishite and namansilite are occasionally observed using microscopy as tiny grains in lipuite (Fig. 2*c*,*d*). Aegirine, hematite and braunite-II are commonly replaced by lipuite (Fig. 2*e*,*f*). The hydrothermal event that formed the observed mineral assemblage has been estimated to be at conditions in the range of 270–420°C at 0.2–1.0 kbar (Kleyenstuber 1984; Gutzmer and Beukes 1996).

Physical and optical properties

Lipuite occurs as platy and granular crystals, 1–3 mm long, or as dark veined agglomerates in the specimens (Fig. 1*a*), in which lipuite shows a dark brown colour with vitreous lustre. The mineral is brittle with uneven fracture. The Mohs hardness is estimated to be ~5 as tested on the specimen by apatite and orthoclase standards, and the streak is red. The measured density by the method of flotation in heavy liquids is 2.83(3) g/cm^3, which is in good agreement with the calculated density of 2.86 g/cm^3. Lipuite is transparent in thin section and features a characteristic red colour with weak pleochroism from bright red to dark red in parallel nicols (Fig. 2*f*). It is biaxial (+) and the interference colour in crossed nicols is also red, probably due to the strong influence of the intrinsic colour as seen in parallel nicols. The measured refractive indices are: α =1.635(1), β = 1.653(1) and γ = 1.670(1), with refractive dispersion of $v > r$. The measured 2V angle is 86(2)°. The calculated compatibility index (0.009) using the constants of Mandarino (1981) yields a superior compatibility with the Gladstone–Dale relationship.

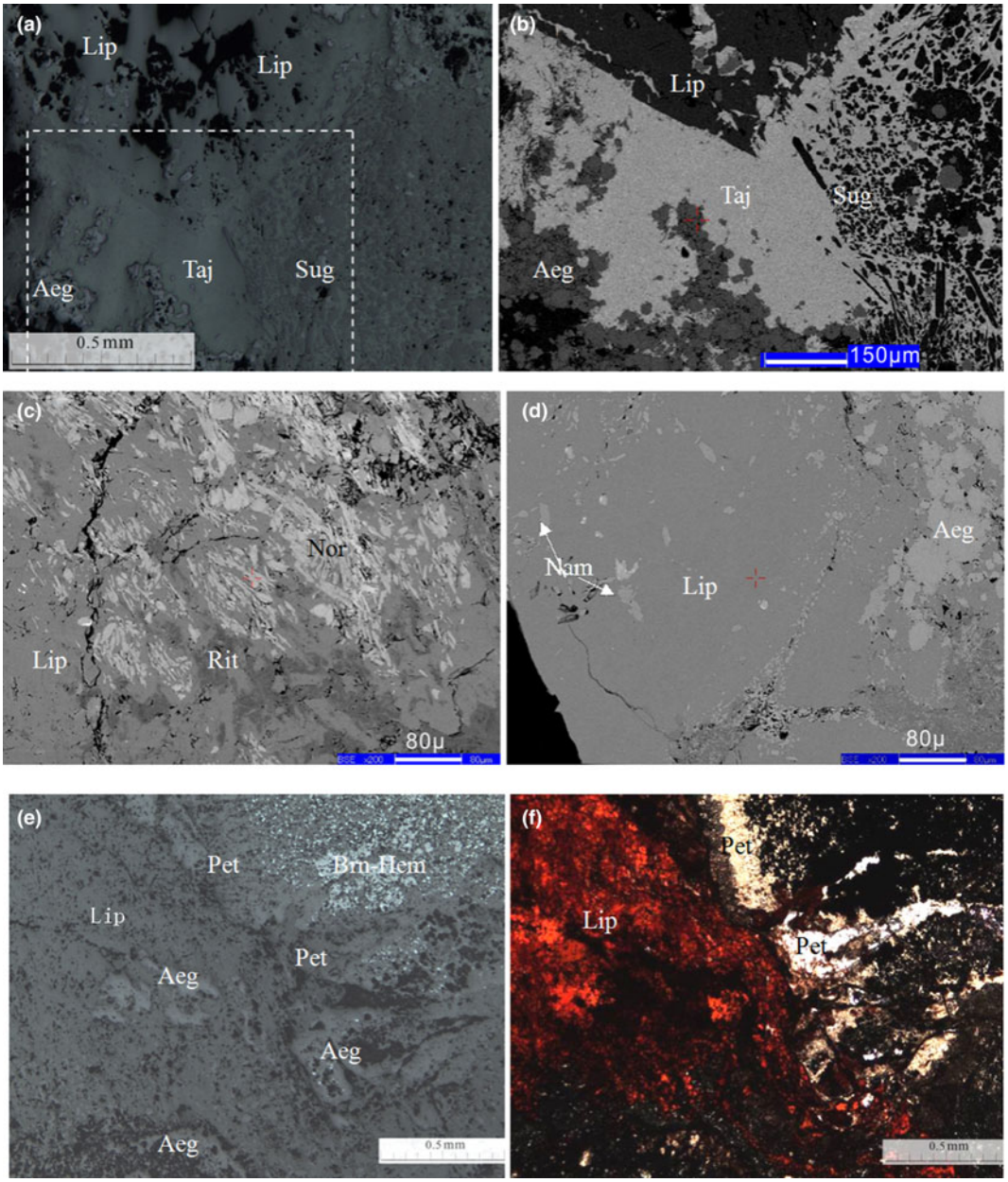

Fig. 2. Photomicrographs and back-scattered electron images (BSE) of lipuite showing the mode of occurrence and optical properties: (*a*) assemblage of lipuite (Lip), sugiilite (Sug) and taniajacoite (Taj) with relics of aegirine (Aeg), parallel nicols, reflected light; (*b*) BSE image of the framed area in (*a*); (*c*) tiny crystals of norrishite (Nor) and richterite (Rit) in lipuite (BSE image); (*d*) namansilite (Nam) and aegirine in lipuite (BSE image); (*e*) lipuite with pectolite (Pet), aegirine, hematite (Hem) and braunite-II (Brn), parallel nicols, reflected light; and (f) characteristic red colour of lipuite, the same view as (*e*), parallel nicols, transmitted light.

Chemical composition

The chemical composition of lipuite was determined on a Shimadzu EPMA-1720 microprobe in the School of Geosciences and Infophysics of Central South University by wavelength-dispersive spectroscopy with operating conditions of accelerating voltage = 15 kV, beam current = 10 nA and beam size = 1 μm. Qualitative analysis revealed dominant Na, K, Mn, Si, P, O and minor Mg and Fe. An intensive X-ray photoelectron spectrometer (XPS) scan of the Li-1s electron was made to determine whether Li was present using a Thermo ESCALAB 250Xi XPS in the Modern Analysis and Testing Centre of Central South University; no peaks were detected in the binding energy range characteristic of Li (53–58 eV). Quantitative analysis was carried out using the following standards (and lines): SiO_2 (Si*K*α); $Ca_5(PO_4)_3F$ (P*K*α); MgO (Mg*K*α); $MnSiO_3$ (Mn*K*α); Fe_2O_3 (Fe*K*α); $NaAlSi_2O_6$ (Na*K*α); and $KAlSi_3O_8$ (K*K*α). The *ZAF3* correction program supplied with the instrument was used for the correction calculation. During analysis, the sample stage was moved around to prevent beam damage to the sample, which was observed to have significantly affected the quantitative analysis. All Fe was assumed to be Fe^{3+} because of the association with trivalent Mn. The theoretical content of 7.74 wt.% of H_2O were used for calculating the number of atoms in the empirical formula. Representative data (Table 2)

Table 2. Chemical composition of lipuite from electron microprobe analyses.

Sample*	$KNa_8Mn^{3+}_5Mg_{0.5}[Si_{12}O_{30}(OH)_4](PO_4)O_2(OH)_2{\cdot}4H_2O$**	lpblock02-01a	lpblock02-01b	lpblock02-01c	lpblock02-01d	lpblock03-01a	lpblock03-02e	lpblock06-02b	lpblock07-04	lpblock08-01	lpblock08-02	Average
Oxide wt.%												
Na_2O	15.23	15.20	15.25	15.59	15.46	15.70	15.54	15.25	15.42	15.33	15.87	15.46
K_2O	2.89	3.23	3.62	3.17	3.25	3.35	3.20	3.07	3.00	3.08	3.15	3.21
Mn_2O_3	24.25	23.18	22.46	22.66	22.51	22.97	22.62	23.20	23.82	23.68	23.15	23.03
Fe_2O_3	–	0.47	0.41	0.50	0.24	0.43	0.13	0.36	0.27	0.38	0.33	0.35
MgO	1.24	0.95	1.18	1.33	1.32	1.07	1.05	0.82	1.10	1.02	1.10	1.10
SiO_2	44.30	44.16	44.03	43.63	43.92	43.72	44.34	44.55	43.14	44.12	43.87	43.95
P_2O_5	4.36	3.80	3.82	4.30	4.41	3.85	3.83	3.73	4.28	4.36	4.28	4.07
Total	92.26	90.99	90.77	91.18	91.11	91.09	90.71	90.98	91.03	91.97	91.75	91.17
H_2O**	7.74	7.74	7.74	7.74	7.74	7.74	7.74	7.74	7.74	7.74	7.74	7.74
Atoms per formula based on total cation = 27.5												
Na	8.00	8.08	8.08	8.22	8.16	8.26	8.21	8.07	8.19	8.07	8.31	8.16
K	1.00	1.13	1.26	1.10	1.13	1.16	1.11	1.07	1.05	1.07	1.09	1.12
Mn	5.00	4.83	4.67	4.69	4.66	4.74	4.69	4.82	4.96	4.89	4.76	4.77
Fe		0.10	0.08	0.10	0.05	0.09	0.03	0.07	0.06	0.08	0.07	0.07
Mg	0.50	0.39	0.48	0.54	0.53	0.43	0.43	0.33	0.45	0.41	0.44	0.44
Si	12.00	12.10	12.03	11.86	11.95	11.86	12.08	12.16	11.81	11.98	11.85	11.97
P	1.00	0.88	0.88	0.99	1.02	0.88	0.88	0.86	0.99	1.00	0.98	0.94
O	46.00	45.86	45.62	45.60	45.71	45.44	45.68	45.95	45.76	45.91	45.51	45.70
H	14.00	14.14	14.11	14.04	14.05	14.05	14.10	14.15	14.13	14.02	13.95	14.07

*Several analyses made on one grain are labelled as 01a, 01b, 01c, 01d etc., and one analysis on a single grain is labelled as 01, 02 etc. without letter a, b etc.
**Ideal formula for comparison; ***Theoretical ideal H_2O contents are used for all analyses; '–' = not present.

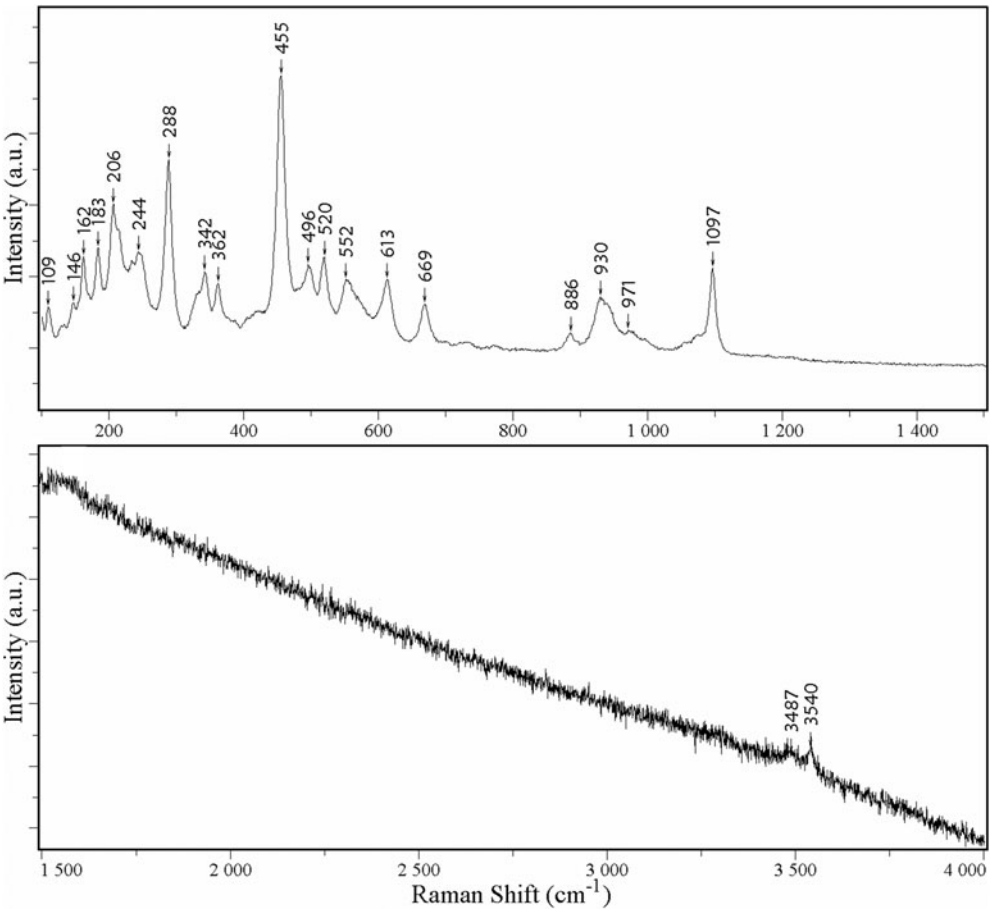

Fig. 3. Raman spectrum of lipuite (sample No. lpblock02-01a in Table 2)

Table 3. Powder X-ray diffraction data for lipuite.

I_{obs}	I_{calc}	d_{obs}	d_{calc}	*h k l*	I_{obs}	I_{calc}	d_{obs}	d_{calc}	*h k l*
40.4	**100.0**	**9.965**	**9.943**	**0 1 1**	10.0	3.3	2.234	2.235	3 3 3
4.8	44.5	8.532	8.548	0 0 2	12.7	9.9	2.214	2.212	4 1 1
21.3	8.7	7.289	7.287	1 1 0	10.0	1.2	2.151	2.152	2 5 0
17.4	18.6	6.713	6.704	1 1 1	9.2	2.5	2.126	2.125	3 2 5
1.6	3.3	5.070	5.070	1 2 0	14.6	4.9	2.112	2.111	4 2 1
28.7	**58.4**	**4.861**	**4.860**	**1 2 1**	**34.5**	**32.8**	**2.086**	**2.084**	**0 4 6**
3.3	1.3	4.541	4.539	2 0 0	4.6	2.1	2.065	2.064	4 2 2
17.8	24.1	4.367	4.360	1 2 2	6.8	9.8	2.048	2.051	1 1 8
3.5	7.8	4.268	4.274	0 0 4	2.6	1.6	2.010	2.012	3 4 3
12.4	19.0	4.129	4.129	2 1 1	9.7	2.6	1.980	1.974	1 6 1
12.3	20.0	4.011	4.009	2 0 2	11.6	10.5	1.966	1.964	3 2 6
10.4	18.8	3.967	3.963	0 3 1	10.9	5.2	1.902	1.904	4 2 4
15.3	18.3	3.810	3.809	2 1 2	8.1	1.1	1.876	1.878	3 1 7
3.1	5.5	3.718	3.717	1 3 0	4.6	5.5	1.848	1.848	2 6 1
27.3	18.0	3.639	3.632	1 3 1	13.8	6.8	1.820	1.820	3 4 5
2.5	2.1	3.567	3.564	2 2 1	6.1	3.3	1.803	1.806	4 2 5
1.7	9.1	3.502	3.502	0 2 4	7.9	5.0	1.796	1.796	5 1 0
21.2	19.0	3.411	3.409	1 3 2	7.5	1.5	1.782	1.786	5 1 1
6.0	7.5	3.354	3.352	2 2 2	3.2	4.0	1.755	1.751	0 4 8
5.8	14.7	3.298	3.293	0 1 5	9.0	4.3	1.740	1.740	5 2 0
3.3	8.0	3.201	3.200	1 0 5	13.2	4.4	1.716	1.715	1 7 0
14.0	19.7	3.112	3.111	2 0 4	3.8	2.6	1.708	1.704	2 6 4
28.5	14.6	3.034	3.032	2 3 0	6.0	4.7	1.662	1.662	3 5 5
4.0	8.9	2.985	2.985	2 3 1	3.3	3.1	1.650	1.651	5 3 1
33.2	**22.0**	**2.938**	**2.937**	**3 1 0**	25.2	10.1	1.629	1.627	4 3 6
100.0	**41.8**	**2.895**	**2.895**	**3 1 1**	6.3	2.5	1.613	1.614	3 4 7
38.1	**17.7**	**2.777**	**2.773**	**2 2 4**	2.8	2.3	1.598	1.597	4 5 3
53.1	**27.2**	**2.713**	**2.712**	**3 2 0**	6.1	3.9	1.555	1.557	2 6 6
10.5	4.6	2.677	2.677	2 3 3	**40.2**	**27.0**	**1.534**	**1.535**	**4 4 6**
24.4	41.3	2.620	2.619	0 3 5	2.0	2.8	1.516	1.516	4 6 0
7.1	4.8	2.583	2.582	1 4 3	12.1	3.3	1.500	1.500	3 5 7
15.4	12.9	2.517	2.516	1 3 5	15.0	6.9	1.493	1.496	4 5 5
31.6	**40.7**	**2.483**	**2.484**	**1 2 6**	5.2	2.6	1.469	1.469	6 2 0
15.0	6.2	2.430	2.430	2 4 2	7.7	5.8	1.434	1.436	4 5 6
9.0	11.3	2.367	2.367	2 1 6	6.1	4.2	1.416	1.417	2 4 10
3.2	4.5	2.338	2.338	1 5 1	3.0	3.8	1.385	1.386	4 6 5
4.5	3.1	2.316	2.316	2 4 3	9.3	5.5	1.374	1.371	2 8 4
30.5	**11.3**	**2.269**	**2.269**	**4 0 0**	6.1	3.2	1.355	1.354	0 9 1

The strongest peaks are given in bold

yield an empirical formula for the average based on total 27.5 cations and according to the structural analysis: $K_{1.12}Na_{8.16}(Mn_{4.77}Fe_{0.07})_{\Sigma 4.84}Mg_{0.44}[Si_{11.97}O_{30}(OH)_4](PO_4)_{0.94}O_2(OH)_2{\cdot}4H_2O$. The ideal formula is $KNa_8Mn_5^{3+}Mg_{0.5}[Si_{12}O_{30}(OH)_4](PO_4)O_2(OH)_2{\cdot}4H_2O$.

Raman spectrum

The Raman spectra of lipuite from 12 spots in 4 polished sections were recorded with a Horiba Labram Aramis Raman spectrometer in the State Key Laboratory of Powder Metallurgy, Central South University. The laser beam (He-Ne laser, 632.8 nm, laser power = 2 mW) was focused to 1 μm with a 100× objective in an Olympus microscope. The time of each scan in the range 100–4000 cm^{-1} was 20 min with a resolution of 2 cm^{-1}. A representative spectrum is shown in Fig. 3. The spectrum is composed of over 21 bands at 109, 146, 162, 183, 206, 244, 288, 342, 362, 455, 496, 520, 552, 613, 669, 886, 930, 971, 1097, 3487 and 3540 cm^{-1}. The bands between 880 and 1097 cm^{-1} can be assigned to P–O and Si–O stretching vibrations of the PO_4 and SiO_4 groups (e.g. Litasov and Podgornykh, 2017; Chakhmouradian *et al.*, 2014). Bands from 430 to 700 cm^{-1} are attributable to O–P–O and O–Si–O bending. The bands below 400 cm^{-1} are associated mainly with rotational and translational modes of PO_4 and SiO_4 tetrahedra, as well as Mn–O interactions and lattice modes. The bands between 3487 and 3540 cm^{-1} are due to O–H stretching.

Table 4. Summary of crystal data and refinement results for lipuite.

Crystal data	
Ideal chemical formula	$KNa_8Mn_5^{3+}Mg_{0.5}[Si_{12}O_{30}(OH)_4](PO_4)O_2(OH)_2{\cdot}4H_2O$
Crystal size	0.06 × 0.05 × 0.05
Crystal system, space group	Orthorhombic, *Pnnm*
Temperature (K)	293
a, *b*, *c* (Å)	9.080(3), 12.222(3), 17.093(5)
V (Å^3)	1897.0(9)
Z	2
Calculated density (g/cm^3)	2.845
μ (mm^{-1})	2.369
Data collection	
Instrument	Bruker X8 APEX2 CCD X-ray diffractometer
Radiation, wavelength (Å)	Mo*K*α, λ = 0.71073
2θ range for data collection	7.34–64.82
Absorption correction	SADABS (Bruker, 2001)
No. of measured, independent and observed [$I > 2\sigma(I)$] reflections	24435, 3483, 2867
R_{int}	0.039
(sin θ/λ)max (Å^{-1})	0.754
Indices range of *h*, *k*, *l*	*h* ± 13, *k* ± 17, *l* ± 25
Refinement	
$R[F^2 > 2\sigma(F^2)]$, $wR(F^2)$, *S*	0.023, 0.060, 1.04
No. of reflections, parameters, restraints	3483, 205, 2
Final R_1, wR_2 factors [$I > 2\sigma(I)$]	0.023, 0.055
Final R_1, wR_2 factors (all data)	0.034, 0.059
Goodness-of-fit	1.036
$\Delta\rho_{max}$, $\Delta\rho_{min}$ (e^- Å^{-3})	0.60, −0.51

X-ray crystallography and structure determination

The powder X-ray diffraction data were collected on a Rigaku D/Max Rapid IIR micro-diffractometer in School of Geosciences and Infophysics of Central South University at 40 kV and 250 mA using a 0.1 mm collimator and exposure time of 60 min. The diffraction data are listed in Table 3. The refined unit-cell parameters are: $a = 9.0772(6)$, $b = 12.2231(8)$, $c = 17.095(2)$ Å, $V = 1896.7(1)$ Å^3 and $Z = 2$.

Single-crystal X-ray diffraction data of lipuite were collected on a Bruker X8 APEX2 CCD X-ray diffractometer equipped with graphite-monochromatised Mo*K*α radiation in the Department of Geosciences, University of Arizona, and frame widths of 0.5° in ω and 30 s counting time per frame. All reflections were indexed on the basis of an orthorhombic unit cell (Table 4). The intensity data were corrected for X-ray absorption using *SADABS* (Bruker, 2001). The systematic absences of reflections suggest the possible space group *Pnn*2 or *Pnnm*. The crystal structure was solved and refined using *SHELX-2014* (Sheldrick, 2015) based on the space group *Pnnm*, because it yielded better refinement statistics in terms of bond lengths and angles, atomic displacement parameters, and *R* factors. There are two possible models for Mg in lipuite, both resulting in the same *R* factors and partial site occupancies. In Model A, Mg is situated at the (0,0,0) site with ~40% occupancy and exhibits a (4 + 2) coordination (four O2 atoms at 2.051 Å and two O11 atoms at 2.718 Å). This model, nevertheless, produces an enormously elongated displacement ellipsoid along the *a* axis. In model B, Mg occupies a split site at (0.0265, 0.0003, 0) (Table 5), with a (4 + 1) coordination (two O2 atoms at 2.03 Å, two O2 atoms at 2.09 Å, one O11 atom at 2.09 Å, and one O11 atom at 2.956 Å) (Table 6),

Table 5. Atomic coordinates and displacement parameters for lipuite.

Atom	*x*	*y*	*z*	U_{eq}	U^{11}	U^{22}	U^{33}	U^{23}	U^{13}	U^{12}
K	0	½	0	0.0442(3)	0.0873(9)	0.0234(4)	0.0215(5)	0	0	0.0125(5)
Na1	0.29763(8)	0.12561(5)	0.27537(4)	0.0178(1)	0.0212(3)	0.0181(3)	0.0142(3)	−0.0011(3)	−0.0023(3)	−0.0010(3)
Na2	0	0	0.19130(6)	0.0170(2)	0.0226(5)	0.0144(4)	0.0140(5)	0	0	−0.0020(4)
Na3	0.59465(11)	0.26394(8)	0	0.0186(2)	0.0188(5)	0.0139(4)	0.0231(5)	0	0	0.0001(4)
Mn1	0.26832(3)	0.13296(2)	0.08707(1)	0.0084(1)	0.0110(1)	0.0076(1)	0.0066(1)	−0.0002(1)	0.0008(1)	0.0017(1)
Mn2	½	0	0	0.0075(1)	0.0079(2)	0.0077(2)	0.0069(2)	0	0	0.0018(2)
Mg*	0.024(3)	0.000(4)	0	0.045(5)	0.0848(156)	0.0228(16)	0.0277(19)	0	0	−0.006(12)
Si1	0.42163(4)	0.28493(3)	0.41371(2)	0.0076(1)	0.0080(2)	0.0083(2)	0.0066(2)	0.0001(1)	0.0001(1)	−0.0003(1)
Si2	0.14867(4)	0.39630(3)	0.34597(2)	0.0076(1)	0.0081(2)	0.0084(2)	0.0064(2)	0.0000(1)	−0.0001(1)	0.0001(1)
Si3	0.14491(4)	0.34626(3)	0.17262(2)	0.0082(1)	0.0082(2)	0.0083(2)	0.0080(2)	0.0008(1)	−0.0002(1)	−0.0002(1)
P	½	½	0	0.0137(2)	0.0180(4)	0.0105(3)	0.0125(4)	0	0	−0.0020(3)
O1	0.3561(2)	0.2528(12)	½	0.0105(3)	0.0109(7)	0.0148(7)	0.0057(7)	0	0	0.0016(5)
O2	0.0317(1)	0.11608(8)	0.08500(6)	0.0106(2)	0.0110(5)	0.0094(5)	0.0113(5)	0.0003(4)	−0.0001(4)	0.0011(4)
O3	0.4963(1)	0.17293(9)	0.38006(7)	0.0110(2)	0.0116(5)	0.0100(5)	0.0115(5)	−0.0015(4)	−0.0036(4)	0.0001(4)
O4	0.2782(1)	0.30295(9)	0.35833(7)	0.0126(2)	0.0125(5)	0.0122(5)	0.0131(5)	−0.0006(4)	0.0048(4)	−0.0021(4)
O5	0.0276(1)	0.38112(9)	0.41337(6)	0.0121(2)	0.0124(5)	0.0149(5)	0.0090(5)	−0.0017(4)	0.0025(4)	0.0014(4)
O6	0.2767(1)	0.01537(9)	0.16170(6)	0.0111(2)	0.0132(5)	0.0109(5)	0.0093(5)	0.0008(4)	0.0010(4)	0.0022(4)
O7	0.0780(1)	0.36356(8)	0.26052(6)	0.0108(2)	0.0106(5)	0.0129(5)	0.0088(5)	0.0015(4)	−0.0005(4)	−0.0002(4)
O8	0.2577(1)	0.24581(9)	0.16642(7)	0.0124(2)	0.0129(5)	0.0129(5)	0.0113(5)	−0.0028(4)	−0.0010(4)	0.0039(4)
O9H	0.2111(1)	0.46330(10)	0.14592(8)	0.0178(2)	0.0168(6)	0.0142(5)	0.0224(7)	−0.0026(5)	0.0045(5)	0.0048(4)
O10A*	0.4331(3)	0.41001(20)	0.04910(15)	0.0211(5)	0.0260(13)	0.0169(11)	0.0202(13)	−0.0015(10)	−0.0082(10)	−0.0047(10)
O10B*	0.1173(4)	0.05507(21)	0.44263(18)	0.0325(7)	0.0455(18)	0.0181(12)	0.0339(16)	0.0029(12)	0.0253(14)	0.0010(12)
O11	0.2956(2)	0.03534(12)	0	0.0087(3)	0.0094(6)	0.0091(6)	0.0076(7)	0	0	0.0010(5)
O12H	0.2646(2)	0.23735(13)	0	0.0135(3)	0.0209(8)	0.0088(7)	0.0106(8)	0	0	−0.0020(6)
O13W	0.0338(2)	0.12522(11)	0.29737(9)	0.0210(3)	0.0233(6)	0.0170(6)	0.0226(7)	0.0001(5)	0.0035(5)	0.0017(5)
H1	0.272(3)	0.465(2)	0.114(2)	0.04**						
H2	0.309(4)	0.292(3)	0	0.04**						
H3	0.020(3)	0.105(2)	0.343(2)	0.04**						
H4	−0.018(3)	0.176(2)	0.298(2)	0.04**						

*The site occupancies Mg, O10A, and O10B are all 0.5. ** The values for the H atoms are U_{iso} values.

Table 6. Selected bond distances (Å) in lipuite.

K–O3	2.944(1) ×4	Na1–O6	2.372(1)	Si1–O2	1.570(1)
K–O9H	3.177(1) ×4	Na1–O9H	2.398(2)	Si1–O4	1.625(1)
K–O1	3.355(2) ×2	Na1–O8	2.400(1)	Si1–O3	1.633(1)
<K–O>	3.120	Na1–O13W	2.425(2)	Si1–O1	1.638(1)
		Na1–O4	2.596(1)	<Si1–O>	1.617
Mn1–O6	1.923(1)	Na1–O3	2.606(1)		
Mn1–O11	1.923(1)	Na1–O7	2.622(1)	Si2–O5	1.608(1)
Mn1–O8	1.937(1)	<Na1–O>	2.488	Si2–O6	1.611(1)
Mn1–O12H	1.961(1)			Si2–O7	1.645(1)
Mn1–O2	2.159(1)	Na2–O2	2.323(1) ×2	Si2–O4	1.652(1)
Mn1–O5	2.360(1)	Na2–O13W	2.392(2) ×2	<Si2–O>	1.629
<Mn1–O>	2.044	Na2–O6	2.570(1) ×2		
		<Na2–O>	2.429	Si3–O8	1.602(1)
Mn2–O11	1.906(2) ×2			Si3–O9H	1.617(1)
Mn2–O5	2.085(1) ×4	Na3–O1	2.383(2)	Si3–O7	1.634(1)
<Mn2–O>	2.026	Na3–O5	2.385(1) ×2	Si3–O3	1.639(1)
		Na3–O10B	2.404(3) ×2	<Si3–O>	1.623
Mg–O2 ×2	2.03(3)	Na3–O10A	2.458(3) ×2		
Mg–O2	2.09(3) ×2	<Na3–O>	2.411		
Mg–O11	2.51(3)				
Mg–O11	2.956(1)	P–O10A	1.511(2) ×4		
Ave. of 5	2.148	P–O10B	1.560(3) ×4		
Ave. of 6	2.282	<P–O>	1.536		

Table 7. Hydrogen bonds in lipuite.

D–H···*A*	*d*(*D*–H) (Å)	*d*(H···A) (Å)	*d*(D···A) (Å)	∠*DHA* (°)
O9H–H1···O10B	0.78(3)	1.81(3)	2.484(3)	144(3)
O9H–H1···O10A	0.78(3)	1.95(3)	2.689(3)	157(3)
O12H–H2···O10A	0.78(4)	2.01(4)	2.739(3)	154(1)
O13W–H3···O10A	0.83(3)	2.01(3)	2.812(3)	161(3)
O13W–H3···O10B	0.83(3)	2.06(3)	2.790(4)	146(2)
O13W–H4···O8	0.77(3)	2.33(3)	3.026(2)	150(3)
O13W–H4···O7	0.77(3)	2.54(3)	3.008(2)	120(2)

D – donor; *A* – acceptor.

similar to that observed in calcioferrite (Lafuente *et al.*, 2014). This model results in a total Mg site occupancy similar to that in Model A, but a relatively more reasonable displacement ellipsoid. Consequently, Model B is adopted in this study.

All four H atoms were located from the difference-Fourier synthesis. The positions of all atoms were refined with anisotropic displacement parameters, except for H atoms, which were refined with a fixed U_{iso} value of 0.04. For simplicity, the ideal chemistry was assumed during the structure refinements. The final coordinates and displacement parameters of atoms, selected bond distances, and the hydrogen-bond scheme for lipuite are given in Tables 5, 6 and 7, respectively. The crystallographic information files have been deposited with the Principal Editor of *Mineralogical Magazine* and are available as Supplementary material (see below).

Crystal structure description and discussion

The crystal structure of lipuite is characterised by sheets of SiO_4 tetrahedra that are linked together along [010] by K^+, Na^+, Mn^{3+}, Mg^{2+} and P^{5+} cations, as well as hydrogen bonds (Fig. 4). These tetrahedral sheets consist of 14-membered rings of SiO_4 tetrahedra that zigzag along [100] (Figs 4 and 5). Calculation of bond-valence sums (Table 8) indicates that one of the O atoms bonded to Si3 is protonated (O9–H) (Table 6). The two independent Mn^{3+} cations are both octahedrally coordinated and they form five-membered, edge-shared octahedral clusters (Fig. 6) between the SiO_4 tetrahedral sheets. Among three

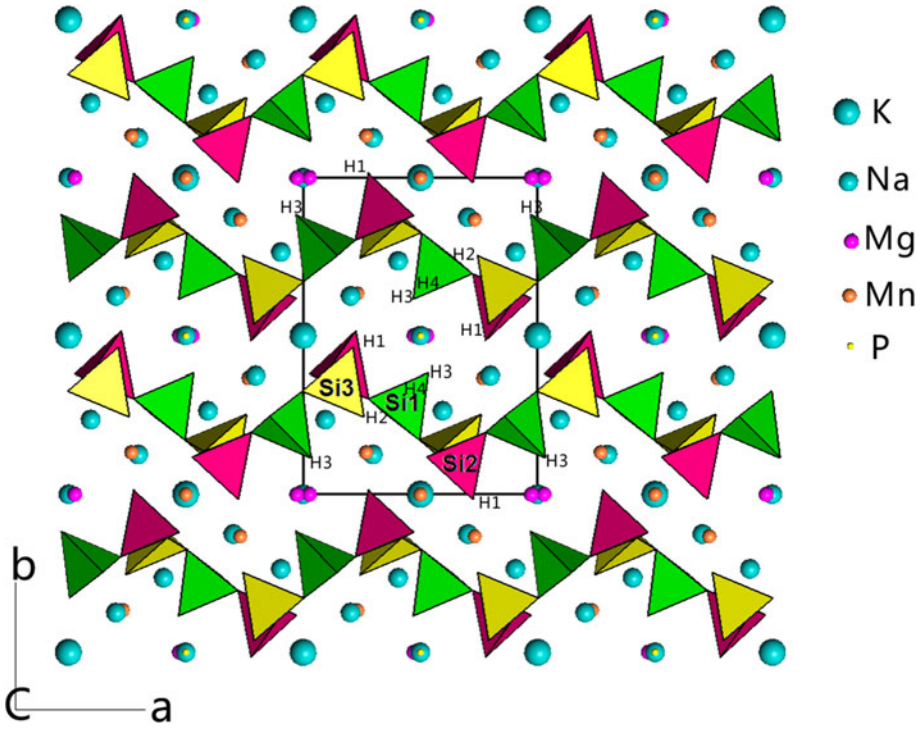

Fig. 4. Crystal structure of lipuite, showing the zig-zagged SiO_4 tetrahedral sheets stacking along the *b* axis, linked together by K^+, Na^+, Mn^{3+}, Mg^{2+} and P^{5+}, which are represented by larger turquoise, smaller turquoise, brown, red and small yellow spheres, respectively.

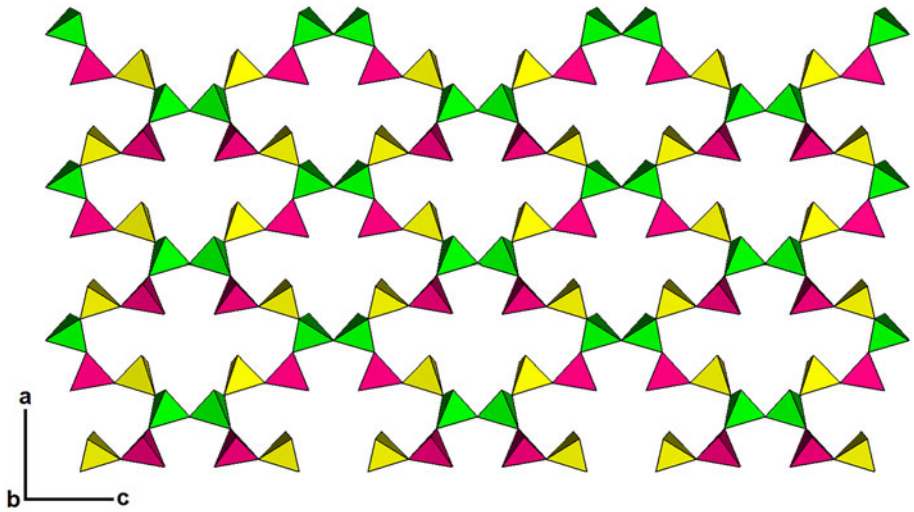

Fig. 5. SiO_4 tetrahedral sheet consisting of 14-membered rings in lipuite: Si1, Si2 and Si3 tetrahedra are represented by green, red and yellow colours, respectively.

distinct Na cations, Na1 and Na3 are 7-coordinated, whereas Na2 is 6-coordinated (Table 4, Fig. 7).

Lipuite represents a unique structure type. Nevertheless, its silicate tetrahedral sheets can be considered a derivative of the silicate sheets in mica, as illustrated in Fig. 8. A silicate sheet consisting of 6-membered rings in mica is shown in Fig. 8*a*. If two tetrahedra are removed from every four 6-membered rings in the sheet, as illustrated in Fig. 8*b*, then we get a silicate sheet that is topologically identical to that in lipuite (Fig. 5). Furthermore, if we replace the two 'removed' SiO_4 tetrahedra with two edge-sharing MnO_6 octahedra, we obtain the polyhedral sheet found in lipuite, which consists of two types of 6-membered rings, with one made of four tetrahedra and two octahedra and the other of five tetrahedra and one octahedra (Fig. 8*c*). The Mn1–O2 bonds are the cause for the kinking of the silicate sheets in lipuite (Fig. 4). Therefore, lipuite may be classified into Class 72 – Two-Dimensional Infinite Sheets with other than six-membered rings in the Dana system or VIII/HX Unclassified Strunz Phyllosilicates in the Strunz system.

Interestingly, the O atoms bonded to P^{5+} are disordered over two distinct sites (O10A and O10B) with each half occupied, giving rise to an apparent distorted cubic coordination for P^{5+}. This disorder may be partly explained by the weak bonding environments around the PO_4 group, which is only bonded to Na^+ and H^+ (hydrogen bonds). Similar disorder of the O atoms in the PO_4 group has also been observed in the eulytine-type compound $Sr_3La(PO_4)_3$ (Barbier *et al.*, 1990). A different kind of disorder of PO_4 groups has been observed in whitlockite-type minerals and

Table 8. Bond-valence sums for lipuite*.

	K	Na1	Na2	Na3	Mn1	Mn2	0.39Mg	Si1	Si2	Si3	P	Sum
O1	0.037 ×2			0.209				0.962 ×2				2.170
O2			0.245 ×2		0.341		0.190 ×4	1.157				1.993
O3	0.111 ×4	0.114						0.975		0.963		2.163
O4		0.117						0.998	0.926			2.041
O5				0.208 ×2	0.197	0.417 ×4			1.041			1.863
O6		0.215	0.126 ×2		0.644				1.038			2.023
O7		0.109							0.948	0.971		2.028
O8		0.200			0.622					1.058		1.880
O9H	0.059 ×4	0.200								1.014		1.273
0.5O10a				0.099 ×2							0.680 ×4	0.779
0.5O10b				0.085 ×2							0.604 ×4	0.689
O11					0.644 ×2	0.675 ×2	0.031 ×2					1.994
O12H					0.577 ×2							1.154
O13w		0.186	0.204 ×2									0.390
Sum	0.756	1.141	1.148	0.992	3.025	3.018	0.822	4.092	3.953	4.006	5.136	

*Parameters for calculations of bond-valence sums were taken from Brese and O'Keeffe (1991).

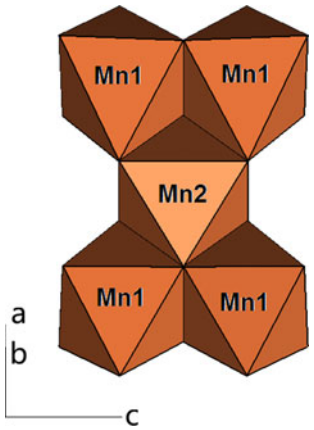

Fig. 6. A five-membered cluster of edge-shared Mn-octahedra in lipuite

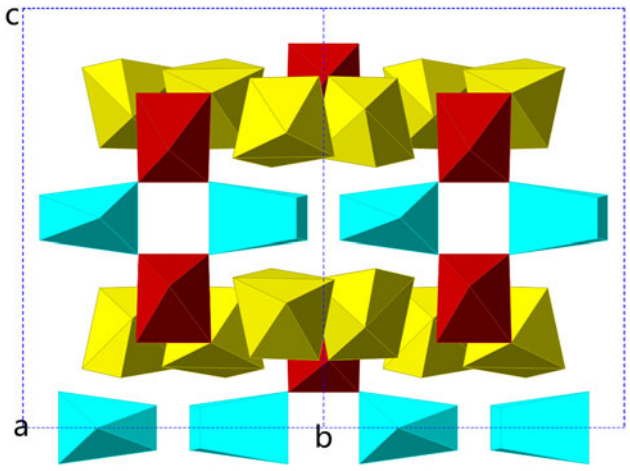

Fig. 7. 7-coordinated polyhedra (Na1 and Na3) and 6-coordinated polyhedra (Na2) in lipuite.

compounds (Zatovsky *et al.*, 2007; Hughes *et al.*, 2008 and references therein), in which the P position in the PO_3OH or PO_3F group is split; it is randomly located either just above or below

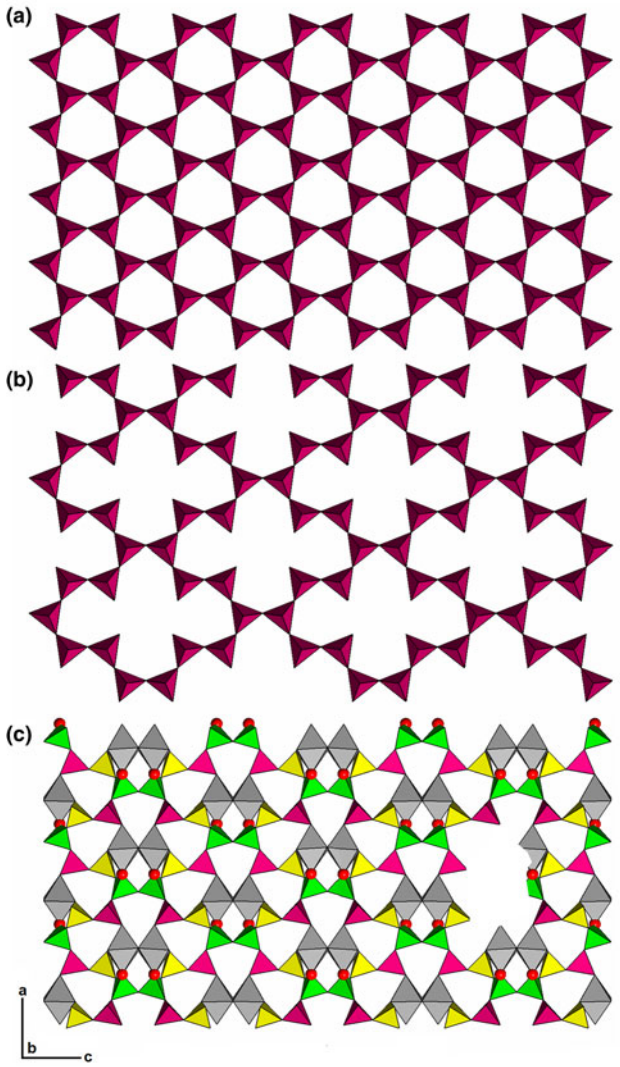

Fig. 8. Comparison of tetrahedral sheets in mica (*a*) and lipuite (*b*) and the location of Mn octahedra (*c*). Si1, Si2 and Si3 tetrahedra are represented by green, purple and yellow colours, respectively, and Mn octahedra by grey.

the midplane, leading the apical OH^- or F^- anion to point either along + **c** or −**c**.

There are two unique OH groups and one unique H_2O in lipuite. The Raman measurements reveal two weak bands in the O–H stretching region, one at 3487 and the other 3540 cm^{-1} (Fig. 3). According to the correlation between O–H stretching frequencies and O–H···O hydrogen bond lengths in minerals (Libowitzky, 1999), these two bands would correspond to an O–H···O distance of 2.8–3.0 Å, agreeing with O–H···O distances for the hydrogen bonds formed by H_2O (Table 5).

Acknowledgements. This study was funded by the Science Foundation Arizona and partial support from National Science Foundation of China (Grant No. 41172042).

Supplementary material. To view supplementary material for this article, please visit https://doi.org/10.1180/mgm.2019.12

References

Armbruster T., Oberhänsli R., Bermanec V. and Dixon R. (1993) Hennomartinite and kornite, two new Mn^{3+} rich silicates from the Wessels mine, Kalahari, South Africa. *Schweizerische Mineralogische und Petrographische Mitteilungen*, **73**, 349–355.

Armbruster T., Gnos E., Dixon R., Gutzmer J., Hejnys C., Dobelln N. and Medenbach O. (2002) Manganvesuvianite and tweddillite, two new Mn^{3+}-silicate minerals from the Kalahari manganese fields, South Africa. *Mineralogical Magazine*, **66**, 137–150.

Barbier J., Greedan J.E., Asaro T. and McCarthy G.J. (1990) Neutron diffraction study of disorder in eulytite-type $Sr_3La(PO_4)_3$. *European Journal of Solid State and Inorganic Chemistry*, **27**, 855–867.

Beukes N.J. (1983) Palaeoenvironmental setting of iron formations in the depositional basin of the Transvaal Supergroup, South Africa. Pp. 131–209 in: *Iron Formations: Facts and Problems* (A.F. Trendall and R.C. Morris, editors). Elsevier, Amsterdam.

Bonazzi P., Bindi L., Medenbach O., Pagano R., Lampronti G.I. and Menchetti S. (2007) Olmiite, $CaMn[SiO_3(OH)](OH)$, the Mn-dominant analogue of poldervaartite, a new mineral species from Kalahari manganese fields (Republic of South Africa). *Mineralogical Magazine*, **71**, 193–201.

Brese N.E. and O'Keeffe M. (1991) Bond-valence parameters for solids. *Acta Crystallographica*, **B47**, 192–197.

Bruker (2001) *SADABS*. Bruker AXS Inc., Madison, Wisconsin, USA.

Cairncross B. and Beukes N.J. (2013) *The Kalahari Manganese Field, the Adventure Continues*. Struik Nature Publishers, Cape Town, South Africa, pp. 384.

Chakhmouradian A.R., Cooper W.A., Ball N., Reguir E.P., Medici L., Abdu Y.A. and Antonov A.A. (2014) Vladykinite, $Na_3Sr_4(Fe^{2+}Fe^{3+})Si_8O_{24}$: A new complex sheet silicate from peralkaline rocks of the Murun complex, eastern Siberia, Russia. *American Mineralogist*, **99**, 235–241.

Dai Y. and Harlow G.E. (1992) Description and crystal structure of vonbezingite, a new $Ca–Cu–SO_4–H_2O$ mineral from the Kalahari manganese field, South Africa. *American Mineralogist*, **77**, 1292–1300.

Dai Y., Harlow G.E. and McGhie A.R. (1993) Poldervaartite, $Ca(Ca_{0.5}Mn_{0.5})(SiO_3OH)(OH)$; a new acid nesosilicate from the Kalahari manganese field, South Africa: crystal structure and description. *American Mineralogist*, **78**, 1082–1087.

de Villiers P.R. and Herbstein F.H. (1967) Distinction between two members of the braunite group. *American Mineralogist*, **52**, 20–30.

Dixon R.D. (1989) Sugilite and associated metamorphic silicate minerals from Wessels mine, Kalahari manganese field. *Geological Survey of South Africa Pretoria Bulletin*, **93**, 47 pp.

Giester G. and Rieck B. (1994) Effenbergerite, $BaCu[Si_4O_{10}]$, a new mineral from the Kalahari Manganese Field, South Africa: description and crystal structure. *Mineralogical Magazine*, **58**, 663–670.

Giester G. and Rieck B. (1996): Wesselsite, $SrCu[Si_4O_{10}]$, a further new gillespite-group mineral from the Kalahari Manganese Field, South Africa. *Mineralogical Magazine*, **60**, 795-798.

Giester G., Lengauer C.L., Pristacz H., Rieck B., Topa D. and Von Bezing K.L. (2016) Cairncrossite, a new Ca-Sr (-Na) phyllosilicate from the Wessels Mine, Kalahari Manganese Field, South Africa. *European Journal of Mineralogy*, **28**, 495–505.

Gutzmer J. and Beukes N.J. (1996) Mineral paragenesis of the Kalahari manganese field, South Africa. *Ore Geology Reviews*, **11**, 405–428.

Hawthorne F.C., Oberti R., Harlow G.E., Maresch W.V., Martin R.F., Schumacher J.C. and Welch M.D. (2012) Nomenclature of the amphibole supergroup. *American Mineralogist*, **97**, 2031–2048.

Hughes J.M, Jolliff B.L. and Rakovan J. (2008): The crystal chemistry of whitlockite and merrillite and the dehydrogenation of whitlockite to merrillite. *American Mineralogist*, **93**, 1300–1305.

Kleyenstuber A.S.E. (1984) The mineralogy of the manganese bearing Hotazel formation of the Proterozoic Transvaal sequence of Griqualand West, South Africa. *Transaction of the Geological Society of South Africa*, **87**, 267–275.

Lafuente B., Downs R.T., Yang H. and Jenkins R.A. (2014) Calcioferrite with composition $(Ca_{3.94}Sr_{0.06})Mg_{1.01}(Fe_{2.93}Al_{1.07})(PO_4)_6(OH)_4{\cdot}12H_2O$. *Acta Crystallographica*, **E70**, 116–117.

Libowitzky E. (1999) Correlation of O–H stretching frequencies and O–H···O hydrogen bond lengths in minerals. *Monatshefte für Chemie*, **130**, 1047–1059.

Litasov K.D. and Podgornykh N.M. (2017) Raman spectroscopy of various phosphate minerals and occurrence of tuite in the Elga IIE iron meteorite. *Journal of Raman Spectroscopy*, **48**, 1518–1527.

Mandarino J.A. (1981) The Gladstone-Dale relationship: Part IV. The compatibility concept and its application. *The Canadian Mineralogist*, **19**, 441–450.

Nyfeler D., Armbruster T., Dixon R. and Bermanec V. (1995) Nchwaningite, $Mn_2^{2+}SiO_3(OH)_2{\cdot}H_2O$, a new pyroxene-related chain silicate from the N'chwaning mine, Kalahari manganese field, South Africa. *American Mineralogist*, **80**, 377–386.

Panikorovskii T.L., Shilovskikh V.V., Avdontseva E.Yu., Zolotarev A.A., Pekov I.V., Britvin S.N. and Krivovichev S.V. (2017) Cyprine, $Ca_{19}Cu^{2+}(Al,Mg,Mn)_{12}Si_{18}O_{68}(OH)_{10}$, a new vesuvianite-group mineral from the Wessels mine, South Africa. *European Journal of Mineralogy*, **29**, 295–306.

Pasero M. (2019) *The New IMA List of Minerals*. http://cnmnc.main.jp/

Peacor D.R., Dunn P.J. and Duggan M. (1983) Sturmanite, a ferric iron, boron analogue of ettringite. *The Canadian Mineralogist*, **21**, 705–709.

Peacor D.R., Dunn P.J. and Nelen J.A. (1990) Orlymanite, $Ca_4Mn_3Si_8O_{20}(OH)_6{\cdot}2H_2O$; a new mineral from South Africa: a link between gyrolite-family and conventional phyllosilicate minerals. *American Mineralogist*, **75**, 923–927.

Rieck B., Pristacz H. and Giester G. (2015) Colinowensite, $BaCuSi_2O_6$, a new mineral from the Kalahari Manganese Field, South Africa and new data on wesselsite, SrCuSi4O10. *Mineralogical Magazine*, **79**, 1769–1778.

Rumsey M.S., Welch M.D., Kampf A.R. and Spratt J. (2013) Diegogattaite, $Na_2CaCu_2Si_8O_{20}{\cdot}H_2O$: a new nanoporous copper sheet silicate from Wessels Mine, Kalahari Manganese Fields, Republic of South Africa. *Mineralogical Magazine*, **77**, 3155–3162.

Sheldrick G.M. (2015) Crystal structure refinement with SHELXL. *Acta Crystallographica*, **C71**, 3–8.

Wahle M.W., Bujnowski T.J., Guggenheim S. and Kogure T. (2010) Guidottiite, the Mn-analogue of cronstedtite: A new serpentine-group mineral from South Africa. *Clays and Clay Minerals*, **58**, 364–376.

Yang H., Downs R.T., Evans S.H. and Pinch W.W. (2013) Scottyite, the natural analog of synthetic $BaCu_2Si_2O_7$, a new mineral from the Wessels mine, Kalahari Manganese Fields, South Africa. *American Mineralogist*, **98**, 478–484.

Yang H, Downs R.T., Evans S.H. and Pinch W.W. (2014) Lavinskyite, $K(LiCu)Cu_6(Si_4O_{11})_2(OH)_4$, isotypic with plancheite, a new mineral from the Wessels mine, Kalahari Manganese Fields, South Africa. *American Mineralogist*, **99**, 525–530.

Yang H., Gu X., Downs R.T. and Xie X. (2015*a*) Taniajacoite, IMA 2014-107. CNMNC Newsletter No. 25, June 2015, page 531; *Mineralogical Magazine*, **79**, 529–535.

Yang H., Gu X., Xie X., van Nieuwenhuizen J.J., Evans S.H. and Downs R.T. (2015*b*) Lipuite, IMA 2014-085. CNMNC Newsletter No. 23, February 2015, page 58. *Mineralogical Magazine*, **79**, 51–58.

Yang H., Gu X., Downs R.T., Evans S.H., van Nieuwenhuizen J.J., Lavinsky R.M. and Xie X. (2019) Meieranite, $Na_2Sr_3MgSi_6O_{17}$, a New Mineral from the Wessels Mine, Kalahari Manganese Fields, South Africa. *The Canadian Mineralogist*, https://doi.org/10.3749/canmin.1800067

Zatovsky I.V., Strutynska N.Y., Baumer V.N., Shishkin O.V., Slobodyanik N.S. (2007) The whitlockite-related phosphate $Ca_9Cr(PO_4)_7$. *Acta Crystallographica*, **E63**, 1180–1181.